Running Head : Distraction and cognitive control on pain

Distraction and cognitive control independently impact parietal and prefrontal neural response to pain

Nicolas Silvestrini[1] & Corrado Corradi-Dell'Acqua[2,3]

[1]Geneva Motivation Lab, Faculty of Psychology and Educational Sciences, University of Geneva, Switzerland

[2] Theory of Pain Lab, Faculty of Psychology and Educational Sciences, University of Geneva, Switzerland

[3] Geneva Neuroscience Center, University of Geneva, Switzerland

Original article,
Title, 13 words
Abstract: 249 words
Introduction: 633 words
Discussion: 1500 words
6 figures
3 Tables

We have no relevant conflicts of interest to declare.

Mailing Address: Nicolas Silvestrini
Dpt. of Psychology, UNI-MAIL, 40, boulevard du Pont d'Arve
CH-1205 Geneva, Tel: +41 22 379 92 68
Email : nicolas.silvestrini@unige.ch

Corrado Corradi-Dell'Acqua
Campus Biotech, 9 Chemin des Mines
CH-1211 Geneva, Tel: +41 22 379 0958
Email : corrado.corradi@unige.ch

Abstract

Pain engages and interacts with high-level cognitive processing. Previous studies documented that distracting someone through a challenging activity leads to hypoalgesia, an effect held to be mediated by parietal and prefrontal structures, who monitor pain-evoked neural response and maintain attention towards task-relevant events. Instead, alternative accounts suggest that challenging activities affect the ability to regulate one's aching experiences, due to partially-common neural substrate between cognitive control and pain at the level the medial prefrontal cortex, which could lead to hyperalgesic after-effects. Here we pulled apart effects of distraction and cognitive control on pain by delivering thermal painful stimulations either *During* or *After* (factor TIME) the engagement of a interfering Stroop paradigm (requiring high cognitive control) or a neutral condition (factor TASK). We found that TIME influenced individual assessment of pain, with less intense ratings associated to the *During* condition. This hypoalgesia was associated with increased activity at the level of dorsolateral prefrontal cortex and the posterior parietal cortex, in interaction with the insular cortex. This was complemented by multivariate pattern analysis who revealed that distraction altered the neural response to pain, by making it more similar to that associated with previous Stroop tasks. Critically, all these effects were observed independently of the nature of the TASK employed which, instead, led to a localized neural modulation at the level of anterior cingulate cortex. Overall, our study underscores the role played by two different faces of human executive functions, which exert independent influence in the neural response evoked by thermal pain.

Introduction

Previous studies established that pain engages and interacts with high-level executive functions (Eccleston and Crombez, 1999; Tracey and Mantyh, 2007; Bushnell et al., 2013; Wiech, 2016). For instance, pain typically disrupts attention and impairs performance *During* cognitive tasks (Moore et al., 2012), while distracting someone through a challenging activity has hypoalgesic effects (Petrovic et al., 2000; Tracey et al., 2002; Valet et al., 2004; Buhle and Wager, 2010; Sprenger et al., 2012). These findings have been interpreted consistently within the neurocognitive model of attention to pain (Legrain et al., 2009), according to which bottom-up nociceptive inputs can engage one's attention, but do so in competition with top-down variables, such as working memory (Eccleston and Crombez, 1999; Legrain et al., 2002; Bingel et al., 2007; Seminowicz and Davis, 2007). At the neural level, regions like the posterior insula, parietal operculum and middle cingulate cortex are held to receive primary thalamic nociceptive inputs (Craig et al., 1994, 2000; Craig, 2003; Segerdahl et al., 2015; Bastuji et al., 2016; Fauchon et al., 2020), and subsequently project to the anterior insula (AI), parietal cortex, and lateral & medial prefrontal structures (Bastuji et al., 2016; Fauchon et al., 2020). This hierarchical architecture fits well the neurocognitive model of attention to pain (Legrain et al., 2009), which suggests that middle cingulate and parieto-insular areas are associated with attention orientation toward pain (bottom-up attention) whereas prefrontal and parietal structures are involved in maintaining attentional load and the processing of goal-relevant stimuli (top-down attention).

Some studies investigated how executing a demanding task could affect also subsequent (but not concurrent) pain experience, with mixed findings. For instance, one research found that pain sensitivity decreased *After* a Stroop task (Hoegh et al., 2019), something that could be

explained as an attentional after-effect, whereby the same mechanisms underlying distraction-hypoalgesia linger also beyond the task's completion. However, other studies found that a Stroop task led to subsequent increase of pain sensitivity (Silvestrini and Rainville, 2013; Silvestrini et al., 2020). In this case, hyperalgesia is interpreted in light of impaired cognitive regulatory processes, as the demanding nature of the Stroop exhausted participants' ability to downplay/regulate the aversive components of the painful experience (Silvestrini and Rainville, 2013; Silvestrini et al., 2020). Indeed, it has been observed that pain and cognitive control disclose distinct but partly co-localized neural networks (Kragel et al., 2018; Silvestrini et al., 2020), which are integrated at the level of the medial prefrontal cortex (Shackman et al., 2011; Silvestrini et al., 2020).

Overall, the literature at hand suggests that affecting different aspects of executive functions might modulate pain in different fashion, with diverted attention decreasing its experience, and exerted cognitive control enhancing subsequent pain. Alternatively, it is possible that the effects of distraction and cognitive control on pain are confounded with one-another, and are mediated by a common prefrontal-parietal network. To address this issue, we run an experiment where we administered noxious thermal stimulations either *During* or *After* an interfering Stroop task (with *high* cognitive control demands) or an easier neutral paradigm, whilst recording pain-related ratings and neural response through fMRI. We predicted decreased sensitivity when pain was administered *During* a task, an effect associated with modulations at the level of prefrontal-parietal structures. Instead, the mixed literature does not allow to make a clear prediction on how pain-responses would be impacted by the nature of the task (Interfering Stroop *vs*. Neutral) at the behavioral level (Silvestrini and Rainville, 2013; Hoegh et al., 2019; Silvestrini et al., 2020), although it is reasonable to assume neural modulations at the level of the

medial prefrontal cortex (Shackman et al., 2011; Silvestrini et al., 2020). The critical question, however, is whether task distraction effects on pain are similar or dissociate from those associated with cognitive control, reflecting the engagement of common *vs*. different facets of individual executive functions.

Methods

Participants and Design

Twenty-nine participants (11 males, mean age = 23.86 ± 4.75 SD) were recruited for the experiment. Participants were volunteers free of self-reported acute or chronic pain, and cardiovascular, neurological, or psychological disease. Furthermore, they signed an informed consent prior to the experiment. This research was conducted in accordance with the Declaration of Helsinki and was approved by the local ethical committee. The study followed a 2 (TIMING: After *vs*. During) x 2 (TASK: Neutral *vs*. Interference) within subject design. We estimated the sample size based on a power analysis assuming a medium effect size (Cohen's d = 0.50, f = .25) with a power of .80 and an alpha of .05, which led to an estimated sample of about 20 participants. We decided to include about 30 participants to consider potential data loss and technical issues. We did not exclude any participants in the statistical analyses and did not recruit additional participants after data analyses.

Painful Thermal Stimulation

A computer controlled thermal stimulator with a 25 x 50 mm fluid-cooled Peltier probe (MSA Thermotest, Somedic, Hörby, Sweden) delivered painful thermal stimulations. The baseline temperature was set to 36°C and each stimulation lasted 16 sec (3 sec of temperature increase,

10 sec of plateau, and 3 sec of temperature decrease). As described below, the temperature of the painful stimulations was adjusted for each participant using a calibration procedure.

fMRI Data Acquisition

A Siemens Trio 3-T whole-body scanner was used to acquire both T1-weighted anatomical images and gradient-echo planar T2*-weighted MRI images with blood oxygenation level dependent (BOLD) contrast. In particular, structural images were acquired with a T1-weighted 3D sequence (repetition time = 1900 msec, inversion time = 900 msec, echo time = 2.27 msec, 1 × 1 × 1 mm voxel size). Instead, the functional sequence was a trajectory-based reconstruction sequence with a repetition time (TR) of 2100 msec, an echo time (TE) of 30 msec, a flip angle of 90 degrees, in-plane resolution 64x64 voxels (voxel size 3 x 3 mm), 32 slices, a slice thickness of 3 mm, and no gap between slices.

Experimental Paradigm

Before the scanning session, participants were seated in a comfortable chair in front of a desktop computer. After a brief oral presentation of the study, participants read and signed the consent form. First, the probe of the thermal stimulator was installed on their right leg in the right lower part of the shinbone and the experiment started by determining individual painful temperature using a staircase procedure. To do so, we applied three series of ascending and descending thermal stimulations. After each stimulation, participants rated pain unpleasantness with a visual analogue scale ranging from 0 (*Not unpleasant at all*) to 100 (*The most unpleasant pain imaginable*). After an initial increase by steps of 2°C, the temperature started decreasing when participants rated pain unpleasantness as more than 70 and increased again when pain

unpleasantness was lower than 50. The last series of ascending and descending stimulations included steps of 1°C. The administered temperatures and associated pain unpleasantness ratings were then displayed on a scatter plot. Based on these data, we selected a temperature that elicited a reliable pain unpleasantness response of about 70 (temperature: *M* = 47.07, *SD* = 1.83, range = 42-51). The selected temperature remained constant throughout the subsequent scanning experiment.

Then, participants received the instructions for the interference and neutral conditions of the counting Stroop task (Bush et al., 1998) and had 16 practice trials in each condition to familiarize themselves with the experimental task and the response key. Participants were informed that they would see sets of one to four identical words presented vertically on the screen. They were asked to report the number of words presented on the screen using the buttons of the keyboard as quickly and accurately as possible, with an emphasis placed on not sacrificing accuracy for speed. Moreover, participants were asked not to blur their vision to make the counting task easier. In the interference condition, the words were the number words “one”, “two”, “three”, and “four”—presented in French (“un”, “deux”, “trois”, “quatre”)—that were always displayed a different number of times than their respective meaning (e.g. two times the words “three”). The interference between reading and counting the words commonly requires cognitive control to override the automatic response of reading and to provide the right answer. In the neutral condition, the presented words were neutral words matched in length with the number words: “an”, “drap”, “table”, and “quille”—which respectively mean in English “year”, “sheet”, “table”, and “skittle”. Words were presented in capital letters in the font Verdana size 24. Trials started with a fixation cross (750ms) followed by the words to count which stayed on

the screen until the participant gave his/her response but not more than 1250ms. During the practice trials, participants received correctness feedback and were asked to answer more quickly if they did not provide an answer within the time limit. Once these practice trials were completed, the thermal stimulator was removed and participants went to the scanner room. They were installed on the scanner bed and the thermal stimulator was installed at the same place on their leg as during the calibration procedure.

Then, participants were moved inside the scanner and two functional scanning runs of 21 min each were conducted, separated by the anatomical scan. Both scanning runs began with a painful thermal stimulation used as a baseline pain induction. After the stimulation, participants rated pain and unpleasantness felt using a cursor displayed on the screen over the visual-analog scales (VAS's) and controlled with the middle and index fingers. The scales ranged from *No pain/Not unpleasant at all* (0) to *The most intense/unpleasant pain imaginable* (100).

Then participants performed four blocks of the counting Stroop task always with a neutral feedback ("response entered"). The feedback appeared for 2 sec minus participants' reaction time, assuring that all trials (3.4 sec) had the same length. Inter-trial intervals varied randomly (750-1500 ms). In the *During* condition, the blocks included 36 trials (2 min 30) and a thermal stimulation was administered at the 32nd trial while the participants were performing the last trials of the task. In the After condition, the blocks included 32 trials (2 min) and a stimulation was administered right after the end of the task. Therefore, the timing of stimulation administration was similar in the *During* and *After* conditions. Each run included the four possible blocks (*During/Interference*, *After/Interference*, *During/Neutral*, and *After/Neutral*), which were

separated by a short break of 12 sec. The order of the blocks was counterbalanced within the runs.

At the end of the task (During condition) or the stimulation (After condition), participants rated pain and unpleasantness felt (total rating time allowed: 24sec) and one item of perceived task difficulty ("How difficult was it for you to achieve the task successfully?"; *Not at all* [0] to *Very difficult* [10]).

The anatomical scan was then completed and the second run started, which was similar to the first run with the four experimental blocks presented in a different order. A total of 10 thermal stimulations were therefore administered during the two scanning runs. Visual stimuli and rating scales were presented on a computer monitor back projected onto a screen and viewed on a mirror placed on the head coil in front of the participant's eyes using a script running in Eprime 2.0 (Psychology Software Tools Inc., Pittsburgh, PA, USA), which also triggered the thermal stimulations.

Data Processing

Behavioural Data

Stroop performance was investigated both in terms of Accuracy and Reaction Time of correct responses. For each subject and condition, the average Accuracy and correct Reaction Times were fed to a paired-sample t-test probing differences between Interference *vs*. Neutral TASK conditions. As for participants' subjective ratings of the thermal stimuli, average Intensity and Unpleasantness values were analysed with Repeated Measures ANOVA, with TIMING (*During vs. After*) and TASK (*Interference vs. Neutral*) as within-subject factors. The analysis was run using R 4.0.4 software (http://cran.r-project.org).

Imaging processing

Preprocessing. Statistical analysis was performed using the SPM12 software (http://www.fil.ion.ucl.ac.uk/spm/), exploiting the preprocessing pipeline from the CONN 21 toolbox (https://web.conn-toolbox.org/ – Whitfield-Gabrieli & Nieto-Castanon, 2012). For each subject, all functional images were realigned to correct for head-movement artefacts, unwrapped to account for geometric distortions related to the magnetic field inhomogeneity, and slice-time corrected to account for temporal delays within the acquisition of a whole brain volume. The Artifact Detection Tools, embedded in the CONN toolbox, were then used for identification of outlier scans in terms of excessive subject motion and signal intensity spikes. Finally, the images were then normalized to a template based on 152 brains from the Montreal Neurological Institute (MNI) with a voxel-size resolution of 2 x 2 x 2 mm, and smoothed by convolution with an 8 mm full-width at half-maximum Gaussian kernel.

First-Level analysis. Preprocessed images from each task were analysed using the General Linear Model (GLM) framework implemented in SPM. For each functional run, we modelled the onset of each of the five thermal stimulations of interest (4 main condition + baseline) with a boxcar function of 10 sec duration starting the moment in which thermode reached the plateau temperature. As for the Stroop task, each of the two conditions (*Interference* and *Neutral*) was delivered through ~2 minutes blocks. Although optimal for testing cognitive control after-effects on pain (Silvestrini and Rainville, 2013; Silvestrini et al., 2020), such long block structure poorly accords with default filtering in SPM (128 sec). To circumvent this, we modelled the onset of each Stroop trial (without distinguishing between *Interference* and *Neutral* blocks) as a delta function, and added an additional predictor of interest in which trials Reaction Times were modulated parametrically. This predictor is expected to capture both differences between Interference and

Neutral Stroop blocks (see results) and within-block fluctuations in performance, and represents a more sensitive test for neural responses of cognitive control which is not confounded with signal low-frequency noise/drifts. This led to 7 predictors for each functional run (5 thermal stimulations, 1 Stroop, 1 Reaction Times parametrical modulation), which were convolved with a canonical hemodynamic response function and associated with their first order temporal derivative. To account for movement-related variance, and other sources of noise, we included the differential movement parameters from the realignment, and dummy variables signalling outlier scans (from the ART toolbox) as covariates of no interest. Low-frequency signal drifts were filtered using a cut-off period of 128 sec, and serial correlation in the neural signal were accounted through first-order autoregressive model AR(1).

Second-level Analyses. Functional contrasts, testing differential parameter estimates images associated with one experimental condition *vs.* the other were then fed in a second level one-sample t-test using random-effect analysis. Effects were identified as significant only if they exceeded a FWE cluster-level correction for multiple comparisons at the whole brain (Friston et al., 1993), with an underlying voxel-level threshold corresponding to $p < 0.001$ (uncorrected).

Functional Connectivity. We complemented the analysis of our study by testing the functional connectivity on the network highlighted by the previous general linear models. As first step, preprocessed data were denoised through the default pipeline in CONN toolbox to remove components in the neural signal which were related to (1) white matter and cerebro-spinal fluid signal (first 15 principal components), (2) estimated subject movement parameters (from preprocessing), (3) the presence of outlier scans (estimated through the ART toolbox during preprocessing), and (4) task-related BOLD signals (in our case, pain-evoked activity and stroop

trials). Data were also band-pass filtered (0.008-0.09 Hz) to account both for slow-frequency fluctuations (such as scanner drift) and well as physiological and residual movement artefacts.

Subsequently, denoised data was fed to ROI-to-ROI connectivity analysis using generalized psychophysiological interaction (gPPI) (McLaren et al., 2012). For the purpose of this analysis we considered the ROIs from Brainnectome parcellation of the human brain (Fan et al., 2016). This allows for a whole-brain fine-grain exploration of the regions involved without any a priori assumption on the implicated network. In particular, we focused on 224 ROIs comprehending the whole atlas, except for the regions 189-210 corresponding to the occipital cortex (Fan et al., 2016, Table 1) which were outside our range of interest. gPPI is a task-dependent functional connectivity analysis computing how strongly the BOLD response time course of two regions are coupled in a given psychological context (in our case, thermal pain). This is implemented though a regression model, whereby the time course of target ROIs is regressed against that of a seed ROI multiplied with the psychological variable. Within the network of interest, every possible combination of seed-target ROIs was considered, thus leading to a 224 x 224 regression coefficients (βs) matrix for each participant, describing the change of coupling between seed and target during pain stimulations. For group-level analysis, individual βs were converted to *z*-scores with Fisher's transformation. Functional contrasts, testing coupling parameters associated with one experimental condition *vs.* the other were then fed in a second level random-effect analysis. To identify conditions of interest, we applied Spatial Pairwise Clustering correction (Zalesky et al., 2012), as implemented in the CONN 21 toolbox. This approach is reminiscent to the cluster-based correction for multiple comparisons for fMRI activation: in this case regression coefficients are clustered together based on hierarchical cluster

analysis based on both functional and spatial criteria (weighting factor 0.5). Clusters of connections exceeding a height threshold corresponding to $p < 0.01$ (uncorrected) are described in terms of *mass* (the sum of the squares of all *t*-values of the surviving paths) which is validated statistically based on the null distribution obtained through 1000 permutations of the original dataset. In particular, clusters were identified as significant if exceeding FDR correction at $p < 0.05$.

Multivariate Pattern Analysis. We also fed the data to multivariate models predictive of subjective pain from brain activity estimated on independent datasets. More specifically, to maximize the comparability with our experiment, we choose the model from Sharvit et al. (2020) derived from datasets obtained with the same device for thermal stimulation and the same MRI scanner than the present study. This is a non-linear model obtained by feeding principal components of brain activity into a Support Vector Regression with a radial basis function kernel. The model's proficiency was established both within the cohort used for the estimation (through cross-validation) and across different experiments (Sharvit et al., 2020). Brain-based estimations of pain unpleasantness was obtained first by reducing each brain-map into the same number of principal components used for the model estimation, and subsequently by feeding the reduced datasets to routines for support vector predictions as implemented in the code available under the Open Science Framework at https://osf.io/jkrvp/. Originally, the model output was an estimate of unpleasantness ranging from 0 (neutral) to 50 (extremely unpleasant). To improve compatibility with the present study, this output was recoded in a 0-100 scale.

In addition, we also considered a multivariate whole-brain model predictive of high (*vs*. low) demands in a Stroop task developed by Silvestrini et al. (2020), obtained through linear

Support Vector Classification. This last model is described in terms of a weight-map with values in each brain coordinate describing the relative linear contribution to the prediction. The brain-based estimation of Stroop demand was obtained as the dot-product of the brain activity from our study with that of the weight maps, as implemented in the code available at the following repository: https://github.com/canlab/Neuroimaging_Pattern_Masks/tree/master/Multivariate_signature_patterns/.

Both models of pain unpleasantness (Sharvit et al., 2020) and Stroop demand (Silvestrini et al., 2020) were applied to pain-evoked parameter estimates in each subject, session and condition. The resulting estimates were then fed to the same analysis scheme used for behavioural measures. We also tested how these models predicted Stroop-evoked activity. For this specific case, we created an *ad hoc* first-level model where we modelled the trials with longest responses in each session separately from those with the most rapid reactions. We then applied both models to the parameter estimates associated with Long and Short Reaction Times and assessed potential differences in the output through paired sample t-test.

Results

Behavioural Responses

Stroop performance

Participants' Accuracy and correct Response Times were analysed as function of the two main TASK conditions. We confirmed that participants were both less accurate (95% *vs*. 94%, $t_{(28)}$ = -2.32, p = 0.028, Cohen's d = -0.44) and slower at responding correctly (629.47 *vs*. 649.34 ms, $t_{(28)}$ = 4.48, p < 0.001, d = 0.83) during the Interference, as opposed to the Neutral condition (see Figure 1A-B).

Thermal Ratings

We analysed thermal ratings through a factorial design, with TIMING (*During vs. After*) and TASK (*Interference vs. Neutral*) as factors of interest. This analysis led to a main effect of TIMING (Pain Intensity: $F_{(1,28)}$ = 7.88, p = 0.014, η_p^2 = 0.22; Unpleasantness: $F_{(1,28)}$ = 6.25, p = 0.018, η_p^2 = 0.19), whereby individuals felt painful temperatures as less intense (69.02 vs. 71.84) and unpleasant (66.17 *vs*. 69.01) while being engaged in the task, rather than in a subsequent time (see Figure 1C-D). No significant modulation of TASK was found, neither as main effect nor in interaction with TIMING ($F_{(1,28)} \leq 1.40$, $p \geq 0.246$). Overall, our data confirm previous evidence of distraction-based hypoalgesia, whereby individuals consider pain less intense and unpleasant while actively engaged in a task. Instead, pain subjective reports were not influenced by the control demands of the task neither when this was concurrent or preceded the noxious stimulations.

Neural Responses

Stroop performance

To identify the network implicated with the demands of the Stroop task, we ran a linear regression searching for regions whose activity increased monotonically with the Reaction Times. Consistently with a wide range of studies employing Stroop (Laird et al., 2005; Hung et al., 2018), and other tasks involving cognitive control (Shackman et al., 2011; Hung et al., 2018; Kragel et al., 2018), we implicated a wide network involving the middle cingulate cortex, supplementary motor area, precuneus, anterior insula (AI), dorsolateral prefrontal cortex (DLPFC), posterior parietal cortex (PPC), thalamus, etc (see Table 1 and Figure 2A for more details). To gather a more stringent functional interpretability of this network, we took a model-based approach, and fed our dataset to a predictive model of Stroop high (*vs*. low) demand developed on an independent dataset (Silvestrini et al., 2020). When applied to our data, we confirmed that this model led to a much stronger output for Stroop trials with longer Reaction Times, than those processed rapidly ($t_{(28)} = 5.07$, $p < 0.001$, $d = 0.94$; see Figure 2B). Instead, when considering whole-brain models predictive of pain unpleasantness (Sharvit et al., 2020) we found no differential output between long vs. short Reaction Times in Stroop ($t_{(28)} = 0.69$, $p = 0.497$, $d = 0.13$; see Figure 2C). Overall, the activity patterns evoked by Stroop demands appear to be similar to that of previous tasks testing cognitive control via Stroop (Silvestrini et al., 2020), while at the same time they differ from those implicated in thermal pain (Sharvit et al., 2020).

Baseline Pain

Subsequently, we inspected the neural responses associated with the delivery of painful temperatures. Figure 3A and Table 2 report brain-evoked activity by the baseline stimulation introducing each experimental session (relative to the non-specified parts of the model [implicit

baseline]), and confirm a widespread network involving bilateral operculum, insula (in both posterior and anterior portions), PPC and right inferior frontal gyrus.

Finally, we fed the brain activity evoked by the baseline temperatures with the whole-brain model predictive of pain unpleasantness (Sharvit et al., 2020), and found a stronger output for those subjects/sessions in which pain was delivered through a higher temperature (Pearson's $r = 0.46$, $p = 0.013$; Figure 3B). Hence, although the temperature was optimized at the individual level to account for individual differences in pain sensitivity, these differences in nociceptive intensity were reliably captured by this pain model. Critically, when feeding the same data to a whole brain model for Stroop demands (Silvestrini et al., 2020), a similar positive relationship between predicted outcome and stimulation temperature was observed ($r = 0.44$, $p = 0.017$; Figure 3B). Hence, although pain and cognitive control activity patterns dissociate at the neural level (Kragel et al., 2018; Silvestrini et al., 2020), it is possible to observe the occurrence of both in the neural response evoked by painful stimulations (Silvestrini et al., 2020).

Stroop-related Pain

Effects of distraction. We then tested the degree to which pain-evoked activity was influenced by the Stroop task. More specifically, when analyzing the main effect of TIMING, we found stronger activity *During* (*vs. After*) the Stroop task in the bilateral DLPFC, bilateral PPC and middle temporal gyrus. Further activity was observed at the level of the dorsomedial prefrontal cortex (Figure 4A and Table 2). Please note that, although in the *During* condition pain stimulations and Stroop trials co-occurred, Stroop effects were independently modelled in the first-level analysis by a dedicated predictor. Hence, the effects described here are interpretable

exclusively in terms of additional neural processing to the Stroop evoked by the thermal stimulation. No region displayed stronger activity in the After (vs. During) condition.

We also analyzed the effect of TIMING also from a connectivity point of view. This analysis identified three clusters of connections similarly impacted by the presence of the Stroop task. In particular, we found that the right and left PPC exhibited decreased connectivity with right DLPFC and AI (Figure 4A, green tracks). Additionally, we also found that the right DLPFC showed increased connectivity with the cingulate cortex, in both its' dorsal (dACC) and subgenual aspects (Figure 4A, purple tracks).

Effects of Stroop demands. Subsequently, we analyzed the effect played by TASK in pain-evoked activity, both as a main effect and in interaction with TIMING. When applying rigorous correction for multiple comparisons for the whole brain no effects were observed. However, it should be mentioned that, at a less conservative threshold (corresponding to $p < 0.001$ uncorrected), we found the dorsal anterior cingulate cortex (dACC) implicated in the main effect of TASK (x = 12, y = 38, z = 20, $t_{(28)} = 4.50$, $p < 0.001$ uncorrected, 122 consecutive voxels), with stronger activity when pain was associated to the Interference (*vs*. Neutral) Stroop condition (Figure 5). Furthermore, we investigated the TASK*TIMING interaction but found no suprathreshold activation. Finally, no effects of Stroop demands were found at the level of connectivity, neither when testing the TASK main effect, nor when modelling the TASK*TIMING interaction

Multivariate Patterns. To achieve a more reliable functional interpretation of our results, we fed the pain-evoked response to a whole-brain model predictive of pain unpleasantness

(Sharvit et al., 2020) and Stroop demands (Silvestrini et al., 2020). More specifically, we analyzed the models' output through a factorial design, with TIMING (During *vs*. After) and TASK (Interference *vs*. Neutral) as factors of interest. In both cases we found a main effect of TIMING (Pain Unpleasantness: $F_{(1,28)} = 8.74$, $p = 0.006$, $\eta_p^2 = 0.24$; Stroop Demands: $F_{(1,28)} = 5.53$, $p = 0.026$, $\eta_p^2 = 0.17$). Figure 6 displays the models' output across the different conditions and reveal that, consistently with what found for subjective responses, brain-estimates of Pain Unpleasantness decreased During *vs*. After the task. Instead, brain estimates of Stroop demands during pain showed an opposite trend, as they increased when participants were engaged in the task, rather than subsequent to it. Hence, distraction makes the pain-evoked activity more similar to that of cognitive control patterns. No significant effects were associated with the factor TASK, neither as main effect, nor in interaction with TIMING ($F_{(1,28)} \leq 1.17$, $p \geq 0.289$).

Discussion

We found a functional dissociation in the role played by distraction and cognitive control in pain experience. This was achieved by engaging participants in a Stroop paradigm (or neutral easier task), which either preceded or was concurrent to the delivery of a thermal painful stimulation. Pain ratings were lower *During* vs. *After* the task, consistently with ample research documenting hypoalgesic properties of distraction (Petrovic et al., 2000; Tracey et al., 2002; Valet et al., 2004; Buhle and Wager, 2010; Sprenger et al., 2012). Such effect was associated with an increased activity at the level of prefrontal, parietal and temporal structures. Furthermore, connectivity analysis revealed that distraction was associated with negative coupling between the PPC and DLPFC-AI, possibly reflecting attentional shift from the thermal stimulation to the active task. Finally, multivariate pattern analysis revealed that distraction altered the neural response associated with pain, by making it less similar to that usually associated with thermal stimulations (Sharvit et al., 2020), and more aligned to that associated with Stroop paradigms (Silvestrini et al., 2020). Critically, all these effects were observed independently of whether the TASK employed was an interfering Stroop (with high demands of cognitive-control) or a neutral condition. Instead, cognitive control led only to an increase of neural activity at the level of dACC. Overall, our study underscores the role played by two different faces of human executive functions, which exert independent influence in the neural response evoked by thermal pain.

Distraction and pain appraisal

Our findings on the neural network underlying distraction hypoalgesia nicely dovetails the predictions from the neurocognitive model of attention to pain (Legrain et al., 2009), which speculates that PPC (especially the intraparietal sulcus) is associated with individual attentional

set, including maintaining the focus on goal-relevant stimuli while inhibiting information from competing sources of information. This can be observed by the increased PPC activity for the *During* condition (Figure 4A), and its' negative coupling with AI (Figure 4B), possibly reflecting the downplaying of brain portions implicated in appraising and attending one's pain experience. Indeed seminal accounts suggest that pain experience could be best interpreted according to a Bayesian framework, whereby the brain estimates the (posterior) probability of potential body damage, based on the integration of sensory inputs and prior representations (Morrison et al., 2013; Wiech, 2016; Tabor et al., 2017; Ongaro and Kaptchuk, 2019; Sharvit et al., 2019; Tabor and Burr, 2019; Seymour and Mancini, 2020). In particular, it is known that merely highlighting to individuals the painfulness of an upcoming stimulation has hyperalgesic effects (Atlas et al., 2010; Sharvit et al., 2015; Koban and Wager, 2016; Loued-Khenissi et al., 2022), with AI playing a key role integrating top-down information with incoming nociceptive signals (Atlas et al., 2010; Geuter et al., 2017; Fazeli and Büchel, 2018; Sharvit et al., 2018). Consequently, distraction might nullify these top-down influences, by inhibiting pain appraisal in AI, and making one's sensitivity more dependent on the information from bottom-up inputs.

Much less clear is the role played by the prefrontal cortex in our study, as it displays increased neural activity during distraction, although in the connectivity analysis DLPFC behaves similarity to AI by showing negative coupling with parietal structures. Furthermore DLPFC-AI show also increased connectivity with portions of the medial prefrontal cortex, especially dorsal and perigenual cingulate areas. This suggests that, as for PPC, the prefrontal cortex is involved in top-down attentional modulation effects of pain, specifically when balancing a conflict between primary goals and competing painful experiences. However, differently from PPC, its involvement

is closely tied with that of AI, possibly reflecting compensatory attentional processes which are engaged whenever the signal in pain-related structures is high. This interpretation would fit the neurocognitive model of attention to pain which speculates that DLPFC is implicated in maintaining attentional load towards primary goals (Legrain et al., 2009), a process that could be recruited in larger extent the more bottom-up competing pain signals are strong.

Distraction and pain regulation

Alternatively, it has been argued that dorsal and medial portions of the prefrontal cortex play an important role in pain regulation and suppression (Lorenz et al., 2003; Wager et al., 2004; Woo et al., 2015; Koban et al., 2017). In this perspective, previous studies associated distraction hypoalgesia to the activity in periaqueductal gray (Petrovic et al., 2000; Tracey et al., 2002; Valet et al., 2004) and descending spinal mechanisms (Sprenger et al., 2012), which in turn are modulated by the prefrontal structures (Valet et al., 2004; Sprenger et al., 2015; Tinnermann et al., 2017). It is in principle possible that our prefrontal activity associated with distraction reflects regulatory processes for pain similar to those observed in previous research. It remains unclear, however, why these mechanisms would be enhanced during the performance of a competing (distracting) task. It could be argued that the Stroop triggers cognitive processes for handling conflicting information which are similar to those associated with pain regulation/control. This would fit the outcome of the multivariate pattern analysis, where independently-validated models of Stroop demands (Silvestrini et al., 2020) can also predict properties of the painful stimulation (Figure 3). However, if this was the case, we should have observed distraction hypoalgesia *only* during the interfering Stroop condition, but *not* during the neutral task. However, as distraction affects pain *regardless* of the nature/complexity of the task involved, we

favour our previous interpretation suggesting that hypoalgesia is driven by a parieto-frontal network who prioritize primary goals and inhibits competing sources of information from AI.

Cognitive Control and pain response

When analysing the effects of TASK we found that pain responses in dACC associated with an interfering Stroop (vs. neutral control) were higher, regardless of whether this condition preceded or was concurrent to the pain stimulation (Figure 5). Hence, manipulating cognitive control through the Stroop can influence specific aspects of the pain response independently of the degree of attention involved. Our results fit previous findings who identify dACC as a key hub for the interplay between cognitive control and pain (Shackman et al., 2011; Silvestrini et al., 2020) and, although the two processes could be dissociated within this brain area (Kragel et al., 2018; Silvestrini et al., 2020), they clearly exert a degree of mutual influence at the point that manipulating the former can influence the neural response of the latter (Silvestrini et al., 2020). Importantly, although neutral effects of cognitive control are orthogonal to those associated with attention, they might not be independent from them as, dACC exhibits also enhanced connectivity with DLPFC-AI during distraction. Hence, pain responses in dACC are also influenced by the attentional manipulation, possibly reflecting the intertwined nature between these two faces of human executive functions.

At the behavioural level, we found no effect of Stroop-induced cognitive control on participants' pain sensitivity. This might appear at odds with the literature who found significant modulations, although with different directions (Silvestrini and Rainville, 2013; Hoegh et al., 2019; Silvestrini et al., 2020). It is reasonable to assume that hidden moderators/confounds might have influenced previous results. For instance, we recently found that cognitive control

after-effects in pain are influenced by the intensity of the noxious input, with mild stimulations leading to hyperalgesia but more intense events leading to hypoalgesia (Riontino et al., 2022). Although it is difficult to compare our study to previous given multiple differences in the nature/duration of the noxious event, it is possible that the stimulation adopted here fell within a "medium" range where its' susceptibility to cognitive control after-effects was minimum. Future studies will need to further investigate the effect of cognitive control and pain sensitivity.

Limitations of the study and conclusive remarks

Given the nature of the research question, our experimental design was constrained by long task sessions, each associated with one thermal stimulation (see also Silvestrini and Rainville, 2013; Silvestrini et al., 2020). This made the task-related signal susceptible to low-frequency fluctuations (which was accounted for in the analysis, see methods), whereas pain-related activity was based on limited repetitions, and with no room for a control painless stimulation. Finally, Figure 1C-D shows a strong desensitization between the first (baseline) thermal stimulation and the subsequent ones. We believe that these limitations have little impact on the main conclusions of the study, which proved to be sufficiently sensitive to capture strong thermal-related effects in the neural signal, and associated attentional effects. Furthermore, the neural modulations associated with TIME mirrored closely behavioural measures of pain and unpleasantness. We should acknowledge, instead, that TASK effects might have benefited from a design which was more sensitive and less confounded by the lack of a control and habituation modulations. Future studies shall rectify this.

Keeping these limitations aside, in this study we pulled apart the role of distraction and cognitive control in pain, with the former affecting subjective experience and triggering a

widespread network involving PPC and DLPFC in interaction with AI, and the latter instead affecting specifically dACC. Overall, our study underscores for the first time the independent, and yet concurrent, role played by two different faces of human executive functions in the neural response to pain.

References

Atlas LY, Bolger N, Lindquist MA, Wager TD (2010) Brain mediators of predictive cue effects on perceived pain. J Neurosci 30:12964–12977.

Bastuji H, Frot M, Perchet C, Magnin M, Garcia-Larrea L (2016) Pain networks from the inside: Spatiotemporal analysis of brain responses leading from nociception to conscious perception. Human Brain Mapping 37:4301–4315.

Bingel U, Rose M, Gläscher J, Büchel C (2007) fMRI reveals how pain modulates visual object processing in the ventral visual stream. Neuron 55:157–167.

Buhle J, Wager TD (2010) Performance-dependent inhibition of pain by an executive working memory task. Pain 149:19–26.

Bush G, Whalen PJ, Rosen BR, Jenike MA, McInerney SC, Rauch SL (1998) The counting stroop: An interference task specialized for functional neuroimaging—validation study with functional MRI. Human Brain Mapping 6:270–282.

Bushnell MC, Čeko M, Low LA (2013) Cognitive and emotional control of pain and its disruption in chronic pain. Nat Rev Neurosci 14:502–511.

Craig AD (Bud) (2003) Interoception: the sense of the physiological condition of the body. Curr Opin Neurobiol 13:500–505.

Craig AD (Bud), Bushnell MC, Zhang E-T, Blomqvist A (1994) A thalamic nucleus specific for pain and temperature sensation. Nature 372:770–773.

Craig AD (Bud), Chen K, Bandy D, Reiman EM (2000) Thermosensory activation of insular cortex. Nat Neurosci 3:184–190.

Eccleston C, Crombez G (1999) Pain demands attention: a cognitive-affective model of the interruptive function of pain. Psychol Bull 125:356–366.

Fan L, Li H, Zhuo J, Zhang Y, Wang J, Chen L, Yang Z, Chu C, Xie S, Laird AR, Fox PT, Eickhoff SB, Yu C, Jiang T (2016) The Human Brainnetome Atlas: A New Brain Atlas Based on Connectional Architecture. Cereb Cortex 26:3508–3526.

Fauchon C, Meunier D, Faillenot I, Pomares FB, Bastuji H, Garcia-Larrea L, Peyron R (2020) The Modular Organization of Pain Brain Networks: An fMRI Graph Analysis Informed by Intracranial EEG. Cerebral Cortex Communications 1 Available at: https://doi.org/10.1093/texcom/tgaa088 [Accessed April 22, 2021].

Fazeli S, Büchel C (2018) Pain-Related Expectation and Prediction Error Signals in the Anterior Insula Are Not Related to Aversiveness. J Neurosci 38:6461–6474.

Friston KJ, Worsley KJ, Frackowiak RSJ, Mazziotta JC, Evans AC (1993) Assessing the significance of focal activations using their spatial extent. Hum Brain Mapp 1:210–220.

Geuter S, Boll S, Eippert F, Büchel C (2017) Functional dissociation of stimulus intensity encoding and predictive coding of pain in the insula. Elife 6.

Hoegh M, Seminowicz DA, Graven-Nielsen T (2019) Delayed effects of attention on pain sensitivity and conditioned pain modulation. European Journal of Pain 23:1850–1862.

Hung Y, Gaillard SL, Yarmak P, Arsalidou M (2018) Dissociations of cognitive inhibition, response inhibition, and emotional interference: Voxelwise ALE meta-analyses of fMRI studies. Human Brain Mapping 39:4065–4082.

Koban L, Kross E, Woo C-W, Ruzic L, Wager TD (2017) Frontal-Brainstem Pathways Mediating Placebo Effects on Social Rejection. J Neurosci 37:3621–3631.

Koban L, Wager TD (2016) Beyond conformity: Social influences on pain reports and physiology. Emotion 16:24–32.

Kragel PA, Kano M, Oudenhove LV, Ly HG, Dupont P, Rubio A, Delon-Martin C, Bonaz BL, Manuck SB, Gianaros PJ, Ceko M, Losin EAR, Woo C-W, Nichols TE, Wager TD (2018) Generalizable representations of pain, cognitive control, and negative emotion in medial frontal cortex. Nature Neuroscience 21:283.

Laird AR, McMillan KM, Lancaster JL, Kochunov P, Turkeltaub PE, Pardo JV, Fox PT (2005) A comparison of label-based review and ALE meta-analysis in the Stroop task. Human Brain Mapping 25:6–21.

Legrain V, Damme SV, Eccleston C, Davis KD, Seminowicz DA, Crombez G (2009) A neurocognitive model of attention to pain: behavioral and neuroimaging evidence. Pain 144:230–232.

Legrain V, Guérit J-M, Bruyer R, Plaghki L (2002) Attentional modulation of the nociceptive processing into the human brain: selective spatial attention, probability of stimulus occurrence, and target detection effects on laser evoked potentials. Pain 99:21–39.

Lorenz J, Minoshima S, Casey KL (2003) Keeping pain out of mind: the role of the dorsolateral prefrontal cortex in pain modulation. Brain 126:1079–1091.

Loued-Khenissi L, Martin-Brevet S, Schumacher L, Corradi-Dell'Acqua C (2022) The effect of uncertainty on pain decisions for self and others. European Journal of Pain 26:1163–1175.

McLaren DG, Ries ML, Xu G, Johnson SC (2012) A generalized form of context-dependent psychophysiological interactions (gPPI): A comparison to standard approaches. NeuroImage 61:1277–1286.

Moore DJ, Keogh E, Eccleston C (2012) The interruptive effect of pain on attention. Q J Exp Psychol (Hove) 65:565–586.

Morrison I, Perini I, Dunham J (2013) Facets and mechanisms of adaptive pain behavior: predictive regulation and action. Front Hum Neurosci 7:755.

Ongaro G, Kaptchuk TJ (2019) Symptom perception, placebo effects, and the Bayesian brain. PAIN 160:1.

Petrovic P, Petersson KM, Ghatan PH, Stone-Elander S, Ingvar M (2000) Pain-related cerebral activation is altered by a distracting cognitive task. Pain 85:19–30.

Riontino L, Fournier R, Lapteva A, Silvestrini N, Schwartz S, Corradi-Dell'Acqua C (2022) Cognitive exertion affects the appraisal of one's own and other people's pain. bioRxiv.

Segerdahl AR, Mezue M, Okell TW, Farrar JT, Tracey I (2015) The dorsal posterior insula subserves a fundamental role in human pain. Nat Neurosci 18:499–500.

Seminowicz DA, Davis KD (2007) Pain enhances functional connectivity of a brain network evoked by performance of a cognitive task. J Neurophysiol 97:3651–3659.

Seymour B, Mancini F (2020) Hierarchical models of pain: Inference, information-seeking, and adaptive control. NeuroImage 222:117212.

Shackman AJ, Salomons TV, Slagter HA, Fox AS, Winter JJ, Davidson RJ (2011) The integration of negative affect, pain and cognitive control in the cingulate cortex. Nat Rev Neurosci 12:154–167.

Sharvit G, Corradi-Dell'Acqua C, Vuilleumier P (2018) Modality-specific effects of aversive expectancy in anterior insula and medial prefrontal cortex. Pain 159:1529–1542.

Sharvit G, Lin E, Vuilleumier P, Corradi-Dell'Acqua C (2020) Does inappropriate behavior hurt or stink? The interplay between neural representations of somatic experiences and moral decisions. Science Advances 6.

Sharvit G, Vuilleumier P, Corradi-Dell'Acqua C (2019) Sensory-specific predictive models in the human anterior insula. F1000Res 8:164.

Sharvit G, Vuilleumier P, Delplanque S, Corradi-Dell'Acqua C (2015) Cross-modal and modality-specific expectancy effects between pain and disgust. Sci Rep 5:17487.

Silvestrini N, Chen J-I, Piché M, Roy M, Vachon-Presseau E, Woo C-W, Wager TD, Rainville P (2020) Distinct fMRI patterns colocalized in the cingulate cortex underlie the after-effects of cognitive control on pain. NeuroImage 217:116898.

Silvestrini N, Rainville P (2013) After-effects of cognitive control on pain. European Journal of Pain 17:1225–1233.

Sprenger C, Eippert F, Finsterbusch J, Bingel U, Rose M, Büchel C (2012) Attention modulates spinal cord responses to pain. Curr Biol 22:1019–1022.

Sprenger C, Finsterbusch J, Büchel C (2015) Spinal Cord–Midbrain Functional Connectivity Is Related to Perceived Pain Intensity: A Combined Spino-Cortical fMRI Study. J Neurosci 35:4248–4257.

Tabor A, Burr C (2019) Bayesian Learning Models of Pain: A Call to Action. Current Opinion in Behavioral Sciences 26:54–61.

Tabor A, Thacker MA, Moseley GL, Körding KP (2017) Pain: A Statistical Account. PLOS Computational Biology 13:e1005142.

Tinnermann A, Geuter S, Sprenger C, Finsterbusch J, Büchel C (2017) Interactions between brain and spinal cord mediate value effects in nocebo hyperalgesia. Science 358:105–108.

Tracey I, Mantyh PW (2007) The cerebral signature for pain perception and its modulation. Neuron 55:377–391.

Tracey I, Ploghaus A, Gati JS, Clare S, Smith S, Menon RS, Matthews PM (2002) Imaging Attentional Modulation of Pain in the Periaqueductal Gray in Humans. J Neurosci 22:2748–2752.

Valet M, Sprenger T, Boecker H, Willoch F, Rummeny E, Conrad B, Erhard P, Tolle TR (2004) Distraction modulates connectivity of the cingulo-frontal cortex and the midbrain during pain—an fMRI analysis. Pain 109:399–408.

Wager TD, Rilling JK, Smith EE, Sokolik A, Casey KL, Davidson RJ, Kosslyn SM, Rose RM, Cohen JD (2004) Placebo-induced changes in FMRI in the anticipation and experience of pain. Science 303:1162–1167.

Whitfield-Gabrieli S, Nieto-Castanon A (2012) Conn: A Functional Connectivity Toolbox for Correlated and Anticorrelated Brain Networks. Brain Connectivity 2:125–141.

Wiech K (2016) Deconstructing the sensation of pain: The influence of cognitive processes on pain perception. Science 354:584–587.

Woo C-W, Roy M, Buhle JT, Wager TD (2015) Distinct Brain Systems Mediate the Effects of Nociceptive Input and Self-Regulation on Pain. PLOS Biology 13:e1002036.

Zalesky A, Cocchi L, Fornito A, Murray MM, Bullmore E (2012) Connectivity differences in brain networks. NeuroImage 60:1055–1062.

Acknowledgments

NS was supported by an *Ambizione* grant awarded from the Swiss National Science Foundation (PZ00P1_142458 / 1). CCD was supported by a *Boursier* grant from the Swiss National Science Foundation (PP00P1_183715). This study was conducted at the Brain and Behavior Laboratory (BBL) at the University of Geneva and benefited from the support of the BBL technical staff.

Figure Legends

Figure 1. Behavioural responses. Boxplots and individual data describing (**A-B**) average Accuracy and correct Reaction Times associated with the Stroop Task, and (**C-D**) average Pain Intensity and Unpleasantness ratings associated with the thermal stimulations. For each boxplot, the horizontal line represents the median value of the distribution, the star represents the average, the box edges refer to the inter-quartile range, and the whiskers to the data range within 1.5 of the inter-quartile range. Individual data-points are also displayed as dots. Orange boxes and dots refer to the Stroop Interference condition (and associated thermal stimulations), whereas azure boxes/dots refer to the Stroop Neutral condition, and grey boxes/dots refer to the Baseline stimulation introducing each experimental session. "***" and "*"refer to significant condition differences at $p < 0.001$ and $p < 0.05$ respectively.

Figure 2. Stroop activity. (**A**) Surface rendering showing regions whose activity during the Stroop task increased linearly with the Reaction Times. To improve the readability of this specific plot, regions are displayed at voxel-level FWE correction for multiple comparisons for the whole brain, thus highlighting only brain portions showing the strongest association. (**B-C**) Predictions from whole brain models of Stroop demands (Silvestrini et al., 2020) and pain unpleasantness (Sharvit et al., 2020). Each model is described in terms of whole-brain maps with coordinates highlighted based on their relative importance. For Stroop model, coordinates describe the relative linear positive (orange) or negative (azure) contribution to the prediction. For pain unpleasantness, coordinates are coded exclusively in terms of non-linear contribution (Sharvit et al., 2020). Each

model is also described in terms of its' proficiency at discriminating between Stroop trials with long vs. short response times, as displayed through dedicated boxplots. *DLPFC*: Dorsolateral Prefrontal Cortex; *AI & PI*: Anterior & Posterior Insula; *SMA*: Supplementary Motor Area; *MCC*: Middle Cingulate Cortex; *PPC*: Posterior Parietal Cortex; *pOP*: Parietal Operculum; a.u.: arbitrary units. "***" significant condition differences at $p < 0.001$.

Figure 3. Baseline temperature. (**A**) Surface rendering showing regions associated with the delivery of the baseline thermal event (when contrasted with the non-specified parts of the model [implicit baseline]). All regions displayed survive cluster-level FWE correction for multiple comparisons for the whole brain. *AI & PI*: Anterior & Posterior Insula; *pOP*: Parietal Operculum; *PPC*: Posterior Parietal Cortex; *IFG*: Inferior Frontal Gyrus (**B**) Linear regressions (with confidence interval areas) and individual data describing the predictions from whole brain models of Stroop demands (Silvestrini et al., 2020) and pain unpleasantness (Sharvit et al., 2020) plotted against the stimulation temperature. "*" refers to significant Pearson's r coefficient at $p < 0.05$.

Figure 4. Distraction-related activity. (**A**) Surface rendering showing regions associated with the delivery of thermal stimulation *During > After* the Stroop task. All regions displayed survive FWE correction for multiple comparisons for the whole brain at $p < 0.05$. The parameter estimates from one outlined region of interest are displayed through boxplots and individual data-points. (**B**) Connectivity changes evoked by the delivery of thermal stimulations *During vs. After* the task. Purple tracks refers to increased connectivity *During > After*, whereas green tracks refer to the opposite contrast. The connectivity parameters from the track connecting right parietal cortex to

lateral prefrontal cortex and anterior insula (*cluster 1*) are also displayed through boxplots and individual data-points. "***"refers to a significant main effect of TIMING at $p < 0.001$. *DLPFC & DMPFC*: Dorsolateral & Dorsomedial Prefrontal Cortex; *IFG*: Inferior Frontal Gyrus; *PPC*: Posterior Parietal Cortex; *MTG*: Middle Temporal Gyrus; *AI*: Anterior Insula; *ACC*: Anterior Cingulate Cortex; *TP*: Temporal pole.

Figure 5. Task-demands effects on pain activity. Surface rendering showing regions associated with the delivery of thermal stimulations associated with the *Interference > Neutral* the Stroop conditions. The activations are displayed under a threshold corresponding to $p < 0.001$ (uncorrected). The parameter estimates from the outlined region are displayed through boxplots and individual data-points. "**" and "*" refer to a significant condition differences at $p < 0.01$ and $p < 0.05$ respectively. *dACC*: dorsal Anterior Cingulate Cortex.

Figure 6. Multivariate Pattern analysis of Stroop-related pain activity. Boxplots and individual data describing the predictions from whole brain models of Stroop demands (Silvestrini et al., 2020) and pain unpleasantness (Sharvit et al., 2020), applied to the Stroop-related pain activity from our data. "**" and "*"refer to a significant main effect of TIMING from a Repeated Measures ANOVA at $p < 0.01$ and $p < 0.05$ respectively.

Tables

Table 1

Stroop Task: parametric modulation of Reaction Times. The implicated regions survive FWE correction for multiple comparisons at the cluster level, with an underlying voxel-level threshold corresponding to *p < 0.001*. L and R refer to the left and right hemisphere, respectively. M refers to medial activations.

	SIDE	***Coordinates***			$T_{(28)}$	***Cluster size***
		x	***y***	***z***		
Parametric modulation of Response Times						
Middle Cingulate Gyrus	M	-10	20	30	7.63	
Supplementary Motor Area	M	-4	8	50	8.78	
Precuneus	M	-10	-66	54	9.04	
Posterior Parietal Cortex	L	-38	-32	50	9.55	
Posterior Parietal Cortex	R	44	-36	42	8.71	
Anterior Insula	L	-28	22	2	10.04	
Inferior Frontal Gyrus	L	-50	12	2	6.75	
Caudate	L	-10	4	10	7.66	
Thalamus	L	-10	-18	8	8.27	
Anterior Insula	R	30	26	0	8.49	
Inferior Frontal Gyrus	R	52	12	2	6.07	73685***
Caudate	R	10	6	6	6.68	
Thalamus	R	10	-10	6	9.71	
Dorsolateral Prefrontal Cortex	R	40	36	18	7.18	
Inferior Temporal Gyrus	L	-52	-62	-8	7.85	
Inferior Temporal Gyrus	R	56	-52	-10	7.24	
Inferior Occipital Gyrus	L	-32	-86	0	6.22	
Inferior Occipital Gyrus	R	36	-88	-2	6.28	
Midbrain	M	8	-22	-12	5.78	
Cerebellum	L	-24	-70	-48	7.65	
Cerebellum	R	22	-48	-26	12.26	

*** $p < 0.001$; corrected for multiple comparisons at the cluster level for the whole brain.

Table 2

Thermal stimulations. Regions associated with the delivery of the baseline thermal event (when contrasted with the non-specified parts of the model [implicit baseline]), and with the main effect of TIMING (during > after). All regions, survive FWE correction for multiple comparisons at the cluster level, with an underlying voxel-level threshold corresponding to *p < 0.001*.

	SIDE	***Coordinates***			***$T_{(28)}$***	***Cluster size***
		x	***y***	***z***		
Baseline Thermal Stimulation						
Posterior Insula	L	-30	-18	12	5.75	2175***
Anterior Insula	L	-30	6	12	6.97	
Posterior Insula	R	42	-4	0	5.90	
Anterior Insula	R	38	18	-6	8.20	
Inferior Frontal Gyrus	R	44	46	2	6.24	4408***
Pallidum	R	18	4	-4	4.47	
Caudate	R	16	16	12	4.31	
Posterior Parietal Cortex	L	-58	-42	48	7.03	547**
Parietal Operculum	L	-64	-26	22	4.95	
Posterior Parietal Cortex	R	62	-36	46	5.89	595**
Parietal Operculum	R	56	-26	24	5.27	
TIMING main effect: during > after						
Dorsolateral Prefrontal Cortex	L	-36	18	46	6.84	1466***
Dorsolateral Prefrontal Cortex	R	40	22	32	5.24	527**
Dorsomedial Prefronal Cortex	M	-2	44	30	4.30	345*
Posterior Parietal Cortex	L	-60	-50	36	4.24	
Superior Temporal Gyrus	L	-46	-48	20	5.97	1837***
Middle Temporal Gyrus (*post. part*)	L	-58	-38	-4	7.62	
Superior Temporal Gyrus	R	62	-50	14	5.23	
Middle Temporal Gyrus (*post. part*)	L	54	-28	-6	5.14	700**
Middle Temporal Gyrus *(ant. part)*	R	52	-4	-22	6.02	
Inferior Occipital Gyrus	L	-24	-98	0	14.47	
Inferior Temporal Gyrus	L	-44	-56	-14	5.33	1640***
Cerebellum	L	-20	-84	-32	5.51	
Inferior Occipital Gyrus	R	26	-96	0	9.51	501**

*** $p < 0.001$; ** $p < 0.01$; *$p < 0.05$ corrected for multiple comparisons at the cluster level for the whole brain.

Table 3

ROI-to-ROI connectivity analysis. Change of functional connectivity associated with the main effect of TIMING. The implicated tracks survive Spatial Pairwise Clustering for multiple comparisons (Zalesky et al., 2012). Each cluster, is described in terms of contributing paths, t-test statistic, and global Mass index. The name of each region is drawn from the Brainnectome atlas (Fan et al., 2016, Table 1).

Connection	$T_{(28)}$	Mass
R IFJ → R SPL A7r	-4.78***	184.31
R SPL A7c → R STG A38l	-4.65***	
R SPL A7r → R IFG A44d	-4.40***	
R SPL A7r → R IFJ	-3.83***	
R IFG A44d → R SPL A5l	-3.58***	
R SPL A5l → R IFG A44d	-3.56**	
R STG A38l → R SPL A7c	-3.54**	
R SPL A7c → R IFG A44d	-3.49**	
R SPL A7r → R STG A38l	-3.39**	
R IFG A44d → R SPL A7r	-3.39**	
R SPL A7r → R vAI	-3.01**	
R SPL A7c → R IFJ	-2.80**	
R IFG A44d → R SPL A7c	-2.80**	
R IFJ → R SPL A7c	-2.80**	
L SPL A7r → R IFG A44d	-5.05***	154.59
R IFG A44d → L SPL A7r	-3.74***	
L SPL A7r → R IFJ	-3.56**	
L SPL A5l → R IFJ	-3.41**	
R IFG A44d → L SPL A5l	-3.35**	
R IFG A44d → L SPL A7ip	-3.30**	
L SPL A5l → R IFG A44d	-3.31**	
L SPL A7ip → R IFG A44d	-3.27**	
L SPL A7c → R IFJ	-3.21**	
L SPL A7c → R IFG A44d	-3.18**	
R IFJ → R IFG A44d	-3.10**	
R IFJ → L SPL A7c	-2.93**	
R IFG A44d → L SPL A7c	-2.27**	
R IFG A44d → L ACC A32p	4.07***	147.84
L ACC A32p → R IFG A44d	3.98***	
R IFJ → L ACC A32sg	3.88***	
L ACC A32p → R IFJ	3.86***	
R IFG A44d → L ACC A32sg	3.45**	
R IFJ → L ACC A32p	3.43**	
R IFJ → R ACC A24rv	3.30**	
R IFJ → R ACC A32sg	3.30**	
R IFG A45c → L ACC A32p	3.26**	
L ACC A32p → R IFG A45c	3.25**	
R IFG A45c → L ACC A32sg	3.19**	
R ACC A32sg → R IFJ	2.98**	

Figures

Figure 1

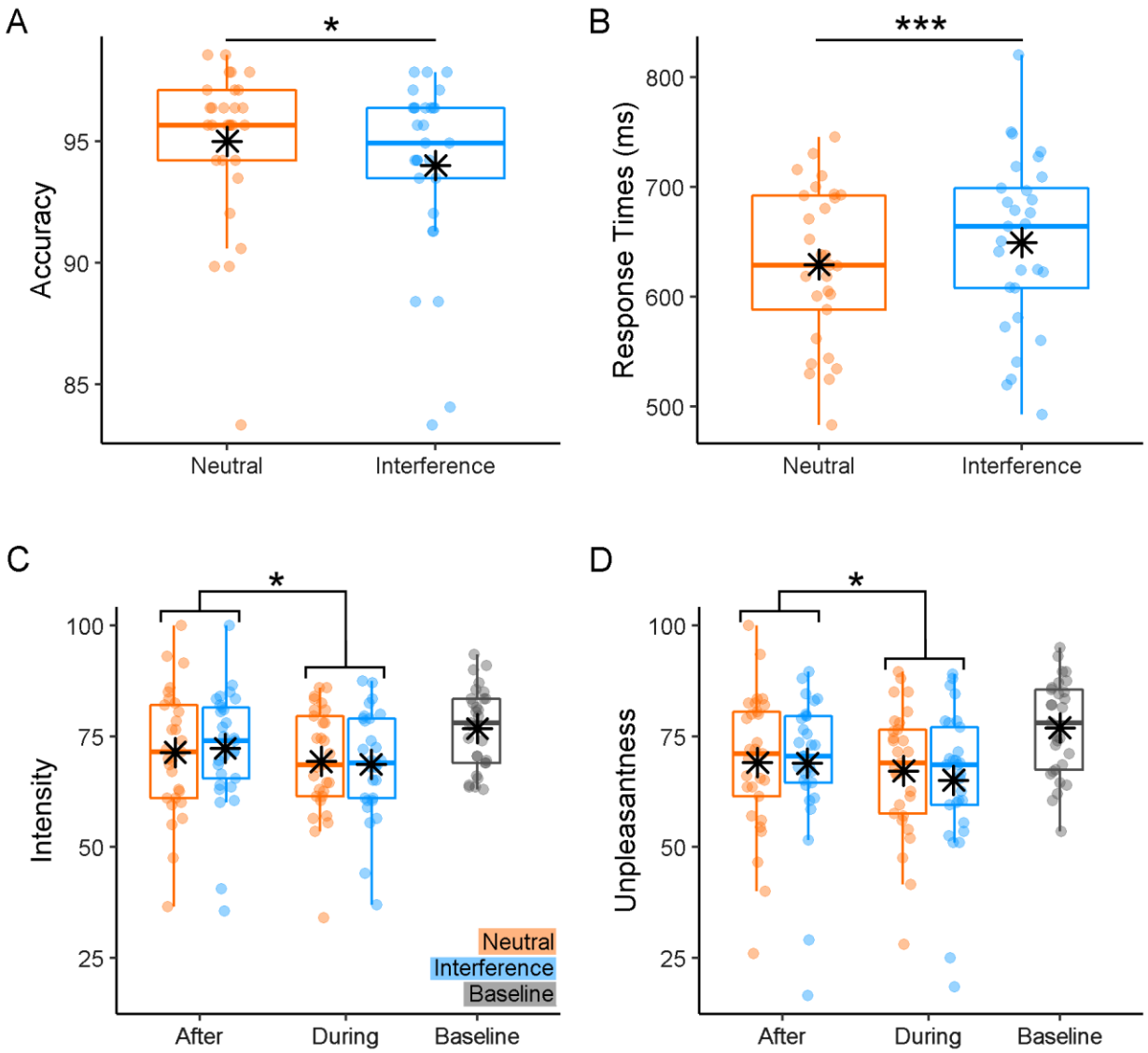

Figure 2

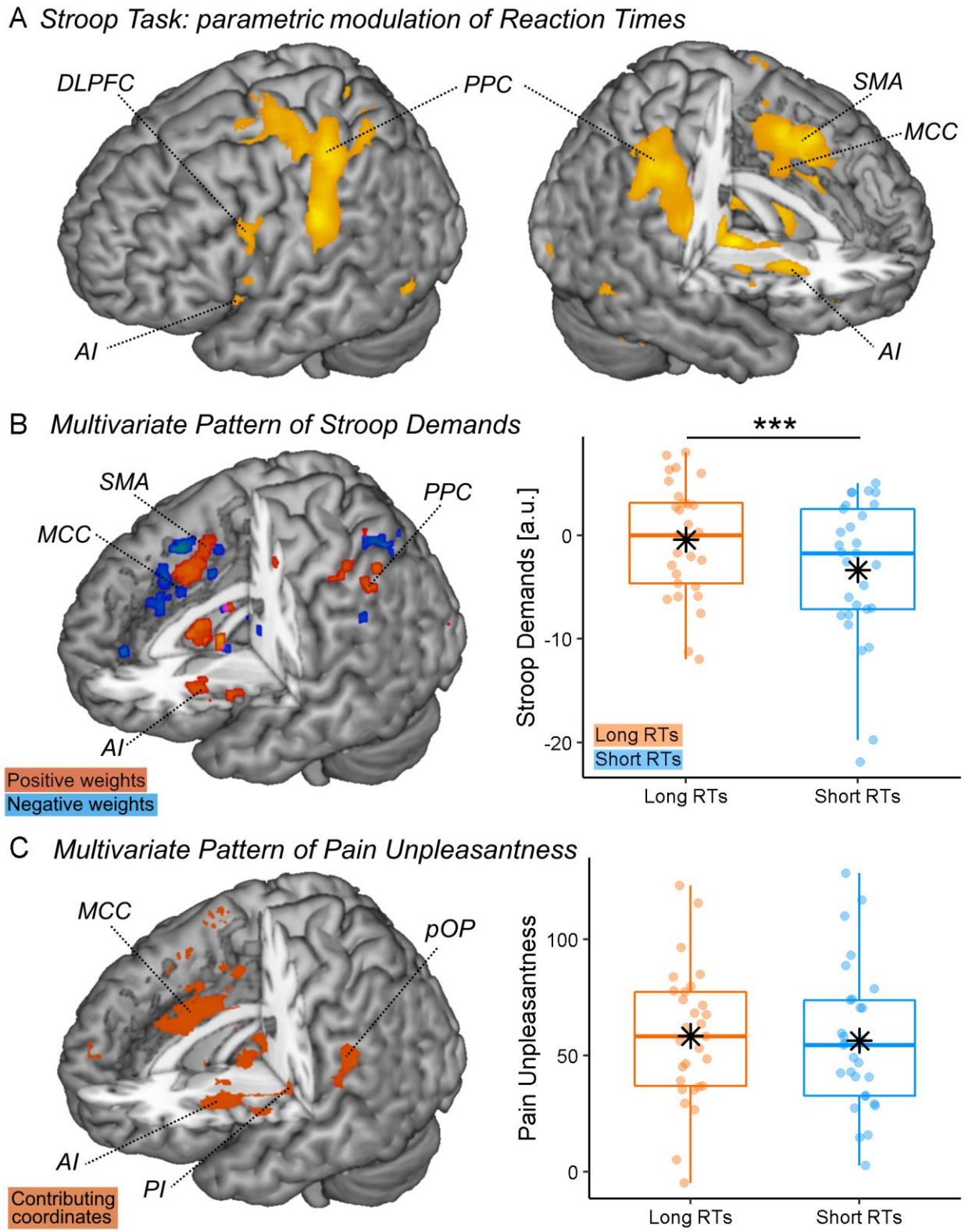
A Stroop Task: parametric modulation of Reaction Times
DLPFC
PPC
SMA
MCC
AI
AI
B Multivariate Pattern of Stroop Demands
SMA
PPC
MCC
AI
Positive weights
Negative weights
***
Stroop Demands [a.u.]
0
-10
-20
Long RTs
Short RTs
Long RTs
Short RTs
C Multivariate Pattern of Pain Unpleasantness
MCC
pOP
AI
PI
Contributing coordinates
Pain Unpleasantness
100
50
0
Long RTs
Short RTs

Figure 3

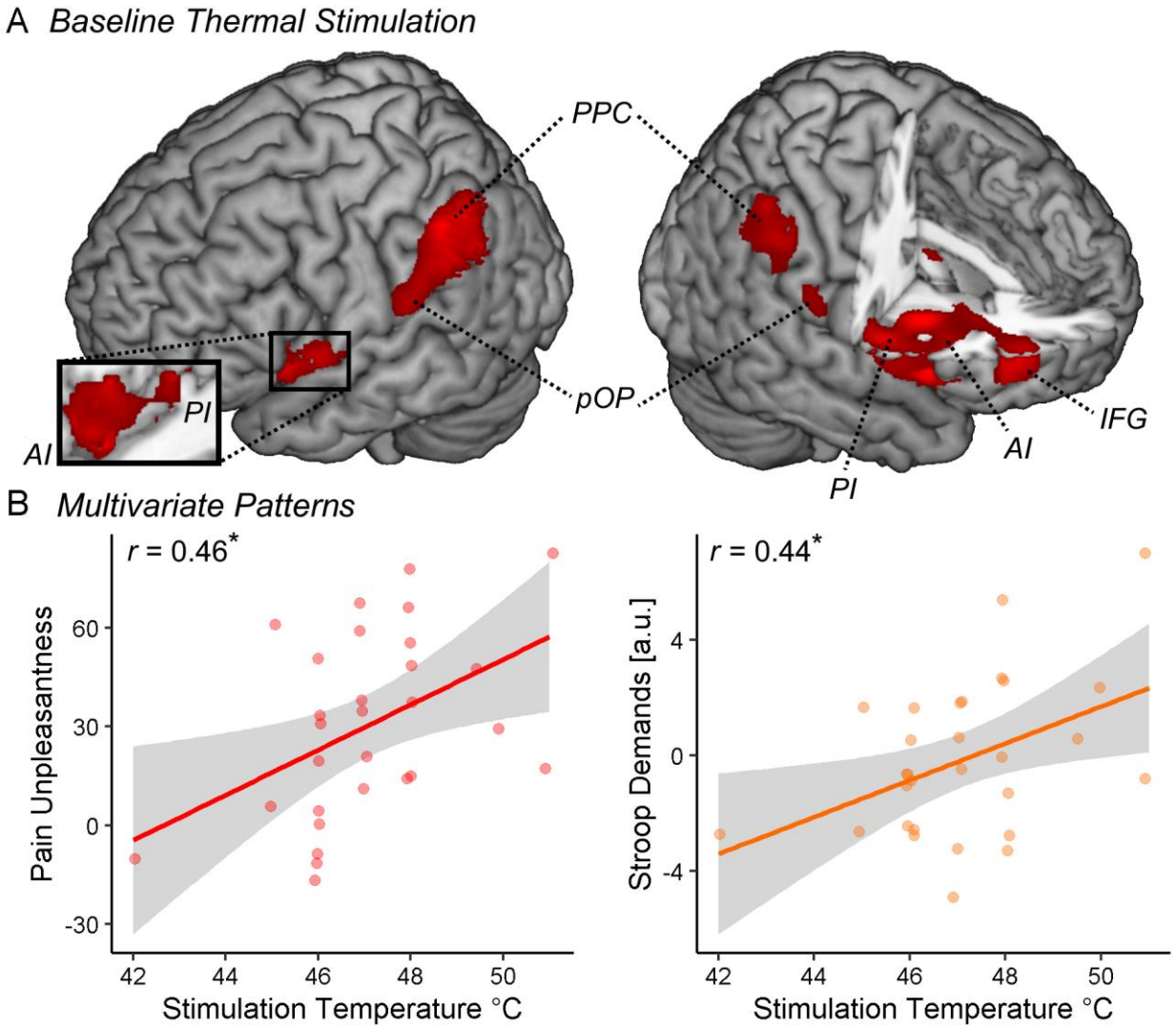
A Baseline Thermal Stimulation
PPC
pOP
PI
AI
IFG
AI
PI
B Multivariate Patterns
r = 0.46*
Pain Unpleasantness
60
30
0
-30
42
44
46
48
50
Stimulation Temperature °C
r = 0.44*
Stroop Demands [a.u.]
4
0
-4
42
44
46
48
50
Stimulation Temperature °C

Figure 4

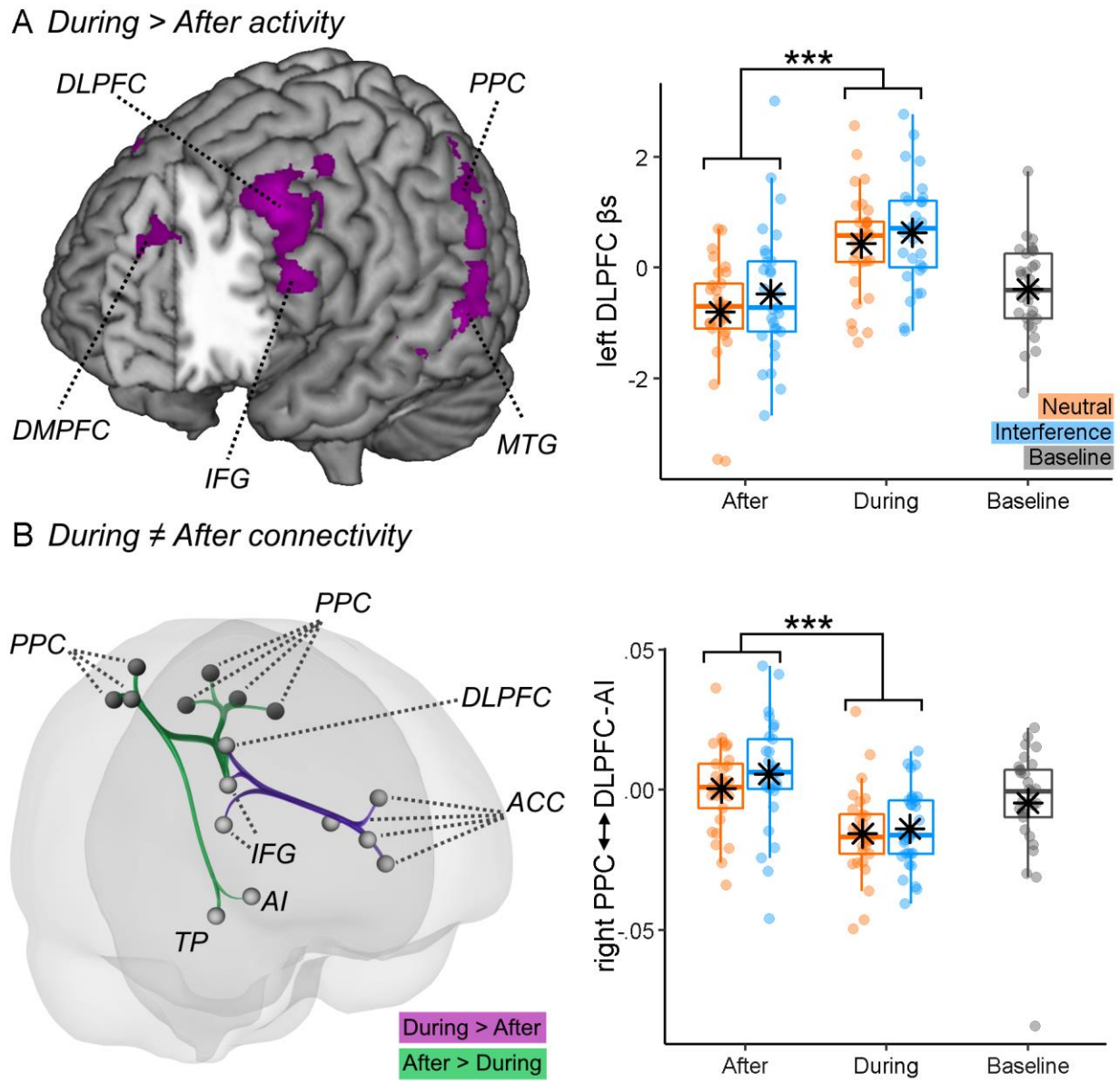
A During > After activity
DLPFC
PPC
DMPFC
IFG
MTG
***
left DLPFC βs
2
0
-2
Neutral
Interference
Baseline
After
During
Baseline
B During ≠ After connectivity
PPC
PPC
DLPFC
ACC
IFG
AI
TP
During > After
After > During
***
right PPC↔DLPFC-AI
.05
.00
-.05
After
During
Baseline

Figure 5

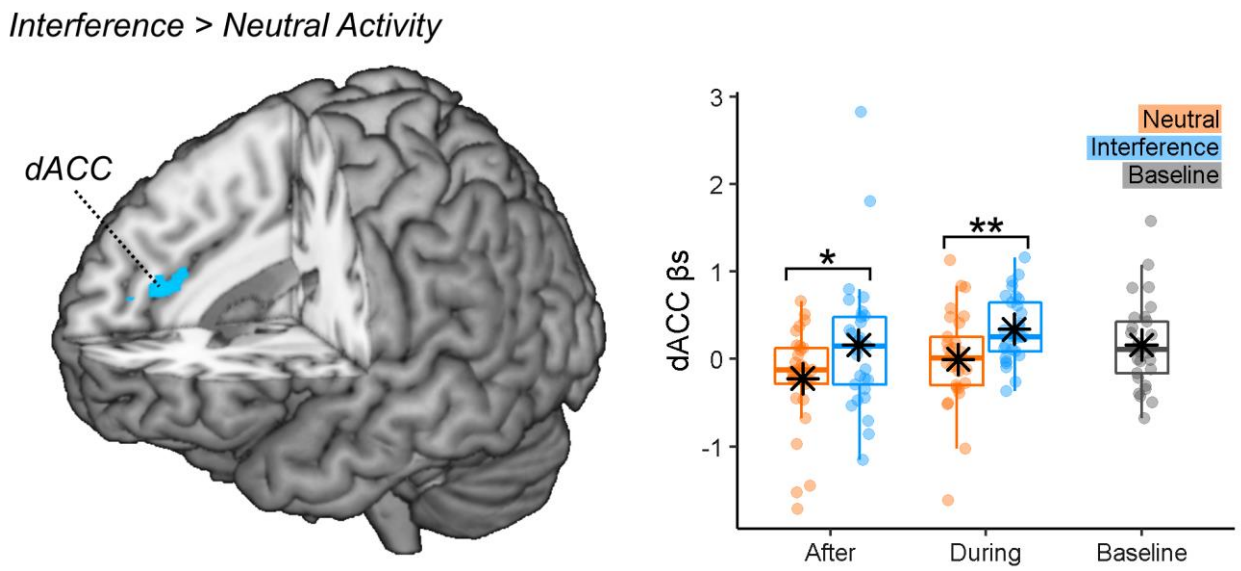
Interference > Neutral Activity
dACC
Neutral
Interference
Baseline
dACC βs
3
2
1
0
-1
*
**
After
During
Baseline

Figure 6

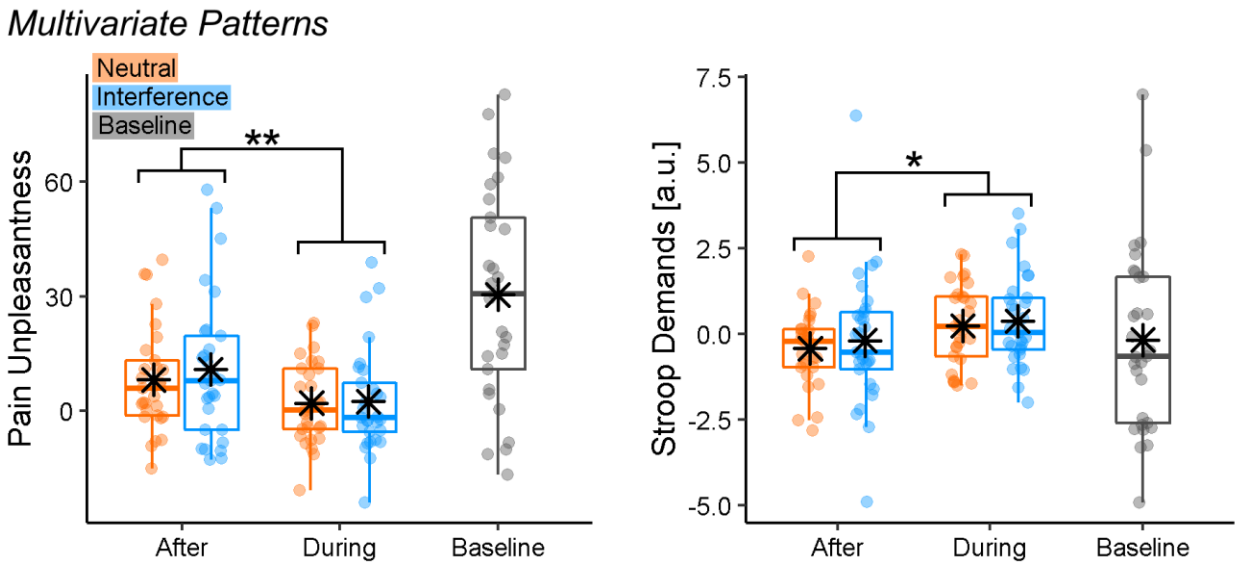
Multivariate Patterns
Neutral
Interference
Baseline
Pain Unpleasantness
60
30
0
**
After
During
Baseline
Stroop Demands [a.u.]
7.5
5.0
2.5
0.0
-2.5
-5.0
*
After
During
Baseline